Heliyon 9 (2023) e21071

Contents lists available at ScienceDirect

Heliyon

journal homepage: www.cell.com/heliyon

Aging-related genes revealed Neuroinflammatory mechanisms in ischemic stroke by bioinformatics

Zhengyu Yao [a,b,1], Jin Jiang [a,b], Yaxin Ju [a,b], Yong Luo [a,b,*]

[a] Department of Neurology, the First Affiliated Hospital of Chongqing Medical University, Chongqing 400016, China
[b] Laboratory Research Center, the First Affiliated Hospital of Chongqing Medical University, Chongqing 400016, China

A B S T R A C T

Ischemic stroke (IS) is a leading cause of disability, morbidity, and mortality globally. Aging affects immune function and contributes to poor outcomes of IS in elderly individuals. However, little is known about how aging-related genes (ARGs) are involved in IS. In this study, the relationship between ARGs and IS immune microenvironment biomarkers was explored by bioinformatics. Two IS microarray datasets (GSE22255, GSE16561) from human blood samples were analyzed and 502 ARGs were identified, from which 29 differentially expressed ARGs were selected. Functional analysis revealed that 7 of these ARGs (*IL1B, FOS, JUN, CXCL5, PTGS2, TNFAIP3* and *TLR4*) were involved in five top enriched pathways (IL-17 signaling pathway, TNF signaling pathway, Rheumatoid arthritis, NF-kappa B signaling pathway and Pertussis) related to immune responses and inflammation. Five hub DE-ARGs (*IL2RB, FOS, IL7R, ALDH2* and *BIRC2*) were identified using machine learning algorithms, and their association with immune-related characteristics was confirmed by additional tests. Single-cell sequencing dataset GSE129788 was retrieved to analyze aging molecular-related features, which was in accordance with microarray datasets. Clustering analysis revealed two subtypes of IS, which were distinguished by their differential expression of genes related to the NF-kappa B signaling pathway. These findings highlight the importance of ARGs in regulating immune responses in IS and suggest potential prevention and treatment strategies as well as guidelines for future research.

1. Introduction

Ischemic strokes (IS) take up to 70 % of all strokes [1]. Every year, nearly 14 million people suffer from stroke; of these 5.5 million will die. Despite the available treatment strategies, stroke remains a major cause of morbidity, disability, and mortality worldwide, thus causing major economic and healthcare burdens (http://world-stroke.org).

A growing body of evidence suggests that the central nervous system (CNS) and immune system communicate bidirectionally and exert profound effects on each other. Briefly, the immune system protects the CNS through the presence of resident immune cells which maintain normal neural function during homeostasis, and through the recruitment of peripheral immune cells during disease states [2,3]. On the other hand, CNS can regulate function of the immune system via the hypothalamic-pituitary-adrenal (HPA) axis, the autonomic nervous system (ANS) and the sympathetic nervous system (SNS) [4,5]. It is noted that neuroinflammation regulated by immune system is critical in IS evolution, which is primarily driven by the excessive activation of immune cells present in the brain like microglia. Subsequently, it follows with an influx of peripheral immune cells of both the innate and adaptive immune systems into the CNS [6]. Numerous studies have demonstrated the critical roles of brain-resident immune cell activation and peripheral immune infiltration in both the acute injury phase and the long-term recovery phase of stroke [7]. However, in contrast, while chronic inflammation is known to be detrimental in stroke cases, it is worth noting that localized inflammation can also play a role in

* Corresponding authorDepartment of Neurology, the First Affiliated Hospital of Chongqing Medical University, Chongqing 400016, China.
E-mail address: luoyong1998@163.com (Y. Luo).
[1] Lead contact: zhengyuyao@stu.cqmu.edu.cn

https://doi.org/10.1016/j.heliyon.2023.e21071
Received 26 March 2023; Received in revised form 26 July 2023; Accepted 13 October 2023
Available online 20 October 2023
2405-8440/© 2023 The Authors. Published by Elsevier Ltd. This is an open access article under the CC BY-NC-ND license (http://creativecommons.org/licenses/by-nc-nd/4.0/).

facilitating the body's innate regenerative mechanisms within the CNS. This natural process acts as a safeguard, preventing the advancement of disease [8].

Aging, which is an inevitable biological process happening to everyone as time elapses, is reported as an important determinant of ischemic stroke risk and outcome, because over 80 % of ischemic strokes occur in people aged 65 years and older [9–11]. As per research findings, there is a greater occurrence of strokes, increased mortality and disability rates among the elderly population. Moreover, older patients exhibit higher vulnerability to complications resulting from thrombolytic treatment in comparison to their younger counterparts [10,12].

Immunosenescence is defined as immune system aging and degeneration, which can be measured by immune function test and immune cell count in blood and immune organs [13]. Immunosenescence can contribute to organ aging, scientists discovered that the composition of circulating and infiltrating leukocytes recruited to the ischemic brain of old male mice after stroke differed significantly from that of young male mice, thus immunosenescence is considered to be a potential contributor to age-related brain injury and neurodegenerative diseases [13,14], and poorer outcomes have been observed due to aging-originated alterations in the immune system of the elderly [15].

However, up to now, studies concerning aging and aging-related genes (ARGs) are mostly concentrated on their influences on the tumor immune microenvironment [16]. Besides, bioinformatic analysis has discovered the relationship between ARGs and other physical diseases concerning the immune microenvironment [17–19], but not IS. According to reports and in line with that, the immune microenvironment of the IS can also exhibit immune-related pathways, immune-related markers, and cellular phenotypes, which are regulated by the immune system [20]. Consequently, it is a reasonable deduction to propose that the process of aging has a notable influence on the regulation of the immune microenvironment within the IS.

In this particular study, a carefully designed set of bioinformatics methodologies were implemented to investigate the association between ARGs and biomarkers of the immune microenvironment in human blood samples obtained from microarray datasets, which can extend our understanding of the relationship between IS development and ARGs and illustrate putative aging-related mechanisms in potential IS onset and progression. The findings of this study may provide guidelines for future experimental research and improve risk assessment-based prevention and treatment of IS.

2. Methods and materials

2.1. Collection and processing of ischemic stroke datasets

The microarray datasets of human blood samples from the GEO database were acquired for our research (https://www.ncbi.nlm.nih.gov/geo/): the GSE22255 (https://www.ncbi.nlm.nih.gov/geo/download/?acc=GSE22255&format=file) [21] and GSE16561 (https://www.ncbi.nlm.nih.gov/geo/download/?acc=GSE16561&format=file) [22] datasets were selected for further analysis. The public dataset GSE22255 contains 20 healthy samples and 20 IS samples, and GSE16561 contains 24 healthy samples and 39 IS samples (Table S1). Subsequently, the R package "inSilicoMerging" [23] was utilized to combine and integrate these two datasets, followed by the application of the ComBat method from the R package "sva" to eliminate batch effects [24]. The process of gene annotation involved assigning gene symbols to gene probes using both the GENCODE and ENSEMBL datasets. Probes that did not correspond to any gene symbols or those that matched multiple symbols were excluded from the analysis. In cases where duplicate gene symbols were present, the gene expression value was calculated as the median value. Besides, In the process of external validation, the microarray dataset GSE58294 (https://www.ncbi.nlm.nih.gov/geo/download/?acc=GSE58294&format=file) [25]

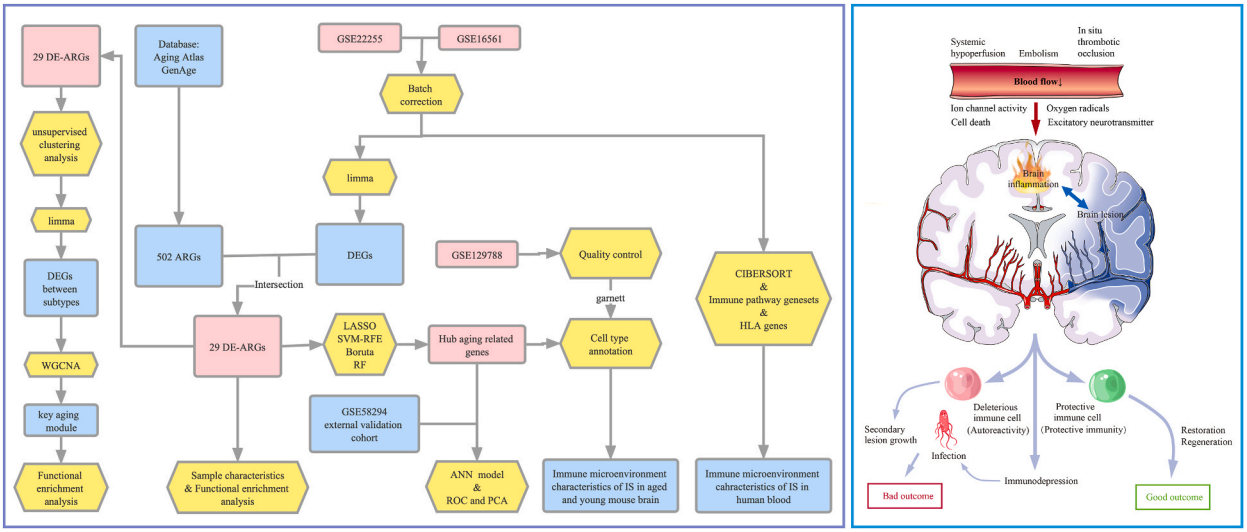

Fig. 1. Workflow of the present study and pathomechanisms of cerebral ischemia.

containing gene expression profiles was utilized. At last, 502 ARGs were derived (Table S2) from two aging databases: “Aging Atlas (https://ngdc.cncb.ac.cn)” [26] and “GenAge (https://genomics.senescence.info)” [27]. The overall process has been displayed accordingly (Fig. 1).

2.2. Identification of differentially expressed ARGs between IS and control

In order to identify the differentially expressed ARGs between IS and control group, the microarray datasets were analyzed by the R package “limma” and genes with p-value <0.05 and $|\log_2$fold-change (FC)$|>0.3$ were selected as differentially expressed genes (DEGs) [28]. By overlapping selected DEGs with ARGs from aging databases, important differentially expressed ARGs (DE-ARGs) were revealed. To visualize the clustering of samples, the "factoextra" package was employed for Principal Component Analysis (PCA) in R (https://cloud.r-project.org/package=factoextra/). The Wilcoxon rank sum test was applied to demonstrate the expression disparities between IS and control, and a heatmap was drawn to display the sample information and DE-ARGs expression levels. At last, the R package "ggplot2" was utilized to calculate and visually represent the correlations among these DE-ARGs.

2.3. Functional enrichment analysis of the DE-ARGs

Subsequently, to figure out the potential enriched functions of the screened DE-ARGs, a protein-protein interaction (PPI) network was built by using the STRING website (https://string-db.org/) and Cytoscape software (V 3.9.1) [29,30]. The metascape (https://metascape.org/) was utilized to perform comprehensive functional gene ontology (GO) analysis, encompassing molecular functions (MF), cellular components (CC), and biological processes (BP), along with KEGG pathway investigation.

2.4. Detection of central ARGs through fusion of four machine learning techniques

To identify central candidate ARGs among the DE-ARGs, we employed four distinct machine learning methodologies individually: LASSO (Least Absolute Shrinkage and Selection Operator) logistic regression, SVM-RFE (Support Vector Machine-Recursive Feature Elimination), Boruta algorithm (Boruta), and Random Forest (RF) algorithms, via the R package “glmnet” [31], “e1071” [32], “Boruta” [33], “xgboost” [34] and “randomForest” [35], respectively. Then, the outputs of these algorithms were overlapped to screen out the central ARGs.

2.5. Development and evaluation of an artificial neural network (ANN) model utilizing IS-associated hub ARGs

For the purpose of categorizing the data of gene expression between IS and control, an ANN model was implemented via the R package “neuralnet” with the central ARGs identified from the four machine learning algorithms. Then, to test the reliability of our predictive model, ROC curve analysis and PCA analysis were utilized. The ROC curve analysis was conducted using the R package "pROC". And the PCA displayed the contribution of each hub ARG.

2.6. Correlation between hub ARGs and immune microenvironment characteristics

To sort out the relationship between the five hub DE-ARGs and the immune microenvironment characteristics of the IS samples. 17 immune pathways from the IMMPORT database (https://www.immport.org) were calculated and 22 distinct infiltrating immunocytes were quantified using the R package "GSVA" and the single-sample gene set enrichment analysis (ssGSEA) algorithm, along with the Cibersortx platform (https://cibersortx.stanford.edu) [36,37], and Wilcoxon rank sum test was also performed to compare the quantification outcomes between IS and control. Moreover, we extracted the HLA gene expression data from the IS datasets, and a comparison was conducted using the Wilcoxon rank sum test. Furthermore, Spearman’s correlation analysis was employed to investigate the potential associations between the five hub ARGs and immunocyte profiles, immune pathways, and HLA gene expression levels, respectively.

2.7. Retrieval and process of single-cell sequencing data

In order to delve deeper into our discoveries at the level of individual cells, we obtained the publicly available Single-cell sequencing (sc-seq) dataset (Table S1) GSE129788 [38] and performed subsequent analyses utilizing R (v4.2.1). The sc-seq data were imported using the function ’CreateSeuratObject’ with parameters ‘min.cells = 3’ and ‘min.features = 200’ in the R package Seurat [39] (v4.3.0). Then, standard workflow was performed: (a) Low-quality cells expressed $\leq$250 genes or $\geq$ 5000 genes or the percent of mitochondrial genes is $\geq$ 5 % were removed [40]. (b) Doublet removal was conducted by the R package DoubletFinder [41] (v2.0.3). (c) To account for the influence of cell cycle variability on cell clustering, we assigned a numerical score representing the cell cycle phase to each sequenced cell. This score was calculated using the ’CellCycleScoring’ function in Seurat, which considered the expression levels of specific genes associated with G1/S and G2/M phases [42]. These calculations were performed using the Seurat object as input. To mitigate the influence of cell cycle heterogeneity, the scores were utilized during data scaling to effectively remove such variability. (d) To standardize the data, the "NormalizeData" function was employed, followed by the identification of the top 2000 variably expressed genes using the "FindVariableFeatures" function. Subsequently, the data was scaled using the "ScaleData" function, principal components (PCs) were computed through the ’RunPCA’ procedure, and ’ElbowPlot’ visualization was employed to

select 20 dimensions as the input for the 'RunUMAP' function. (e) The R package "harmony" was employed for batch correction among different samples [43]. (f) To distinguish the cell clusters, we utilized the FindNeighbors and FindClusters functions, setting the dimensions and resolution parameters to 20 and 0.5, respectively. (g) Cells were annotated using a supervised method termed Garnett [44] that leverages machine learning to classify each of the cell, markers were retrieved from previous literature [45] and Cell Taxonomy database [46], and markers failed to match the data were removed.

2.8. Analysis of aging molecular-related features in single-cell sequencing data

We investigated the ageing molecular-related features in sc-seq data and visualized expression levels of hub genes in various cells using the DotPlot and FeaturePlot functions. Additionally, the aging-related gene sets of Mus musculus were acquired from the GenAge and Aging Atlas databases, and we calculated the scores of the aging signature scores for each cell via the AddModuleScore function, which were then visualized using the FeaturePlot function. Subsequently, we compared the ageing signature scores in old and young groups using the Wilcoxon test. Afterwards, based on the median score of aging signatures, we further divided samples into aging signature-high and aging signature-low subgroups and assessed the correlation between aging signature status and clinical old and

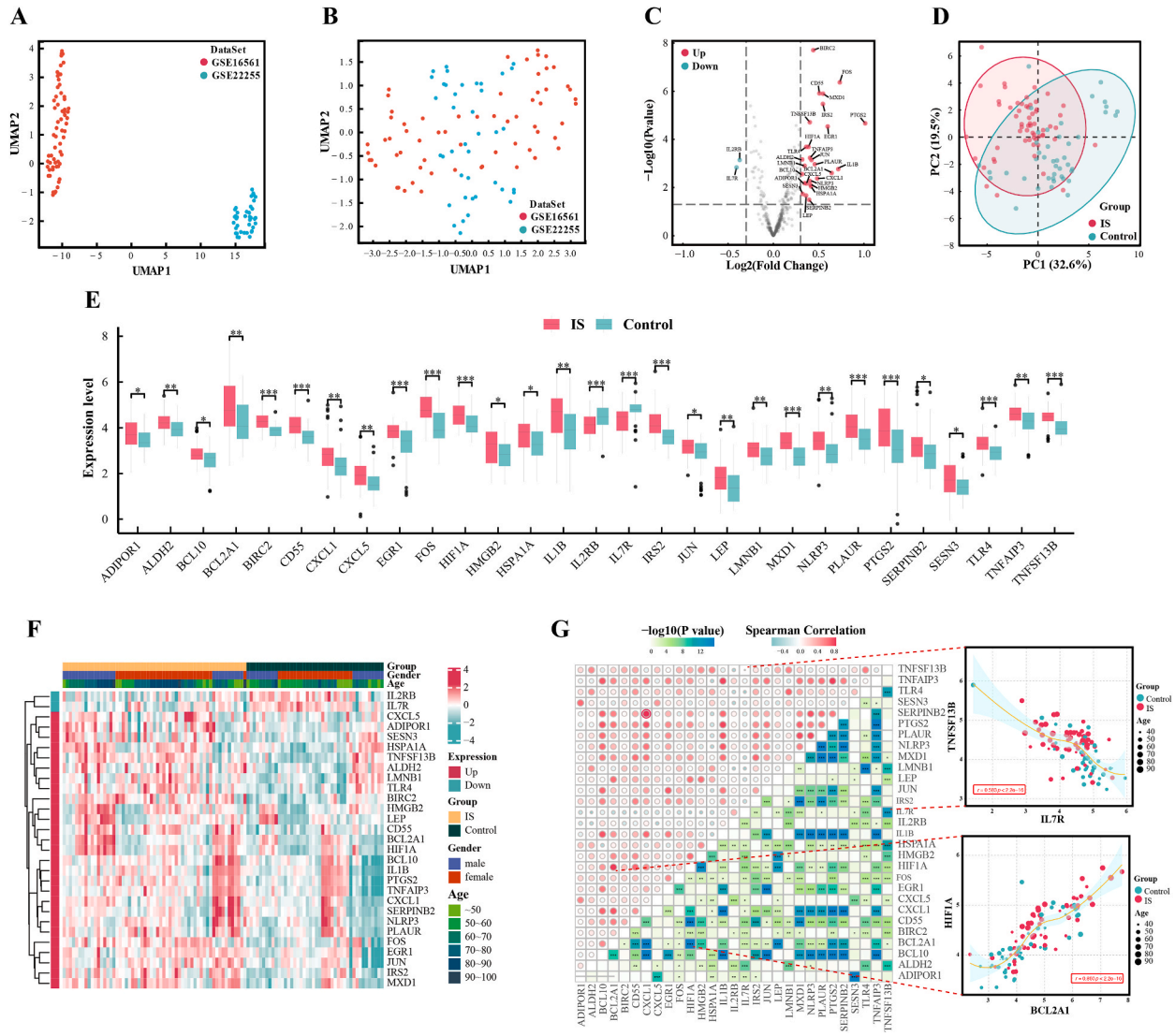

Fig. 2. Data processing and expression patterns of DE-ARGs in IS. (A, B) UMAP plots showed the merge and batch correction of GSE16561 and GSE22255. (C) Volcano plot showed the upregulated and downregulated DE-ARGs in IS compared with control. (D) PCA analysis reveals expression disparities between IS and control groups using 29 DE-ARGs. (E) Expression levels of 29 DE-ARGs were compared via the Wilcoxon rank sum test. (F) Heatmap showed the 29 DE-ARGs expression patterns and clinical information in IS and control. (G) Heatmap showed correlations between the 29 DE-ARGs, greatest correlation of negative and positive were displayed in bubble scatter plots beside. Data are expressed as means ± SD, *: $P < 0.05$; **: $P < 0.01$; ***: $P < 0.001$.

young.

2.9. Identification of aging-related molecular subtypes in IS patients

In order to distinguish different molecular subgroups with distinct gene-expression signatures by a classic method as previously reported [47]. An unsupervised clustering analysis was performed by using the R package "ConsensusClusterPlus". Furthermore, a classification into two aging expression subtypes was accomplished, utilizing the expression profiles of 29 DE-ARGs [48]. To guarantee the robustness of the clustering process, we conducted 1000 iterations, with each iteration including 80 % of the samples. Then we identified the ideal number of clusters by analyzing the cumulative distribution function (CDF) curve of the consensus score. Principal Component Analysis (PCA) was employed to examine the distribution of genes within the subtypes. To evaluate the expression patterns of the 29 ARGs in the two aging-related subtypes, we performed the Wilcoxon rank sum test. Furthermore, we investigate the subtype-associated Reactome pathways and HALLMARKS utilizing the GSVA algorithm [49]. At last, for a supplement, Wilcoxon rank sum test was performed again to compare the quantification outcomes of immunocytes, immune-related pathways and HLA expression levels between distinct subtypes.

2.10. Detection of gene modules associated with aging phenotype

In addition, we aimed to investigate the molecular phenotype characteristics associated with aging, aiming to enhance our understanding of the underlying molecular mechanisms involved in age-related regulatory processes. DEGs ($p < 0.05$) between subtype 1 and subtype 2 were ruled out by the same token, and these DEGs were subjected to the weighted correlation network analysis (WGCNA). The module with the most significant correlation coefficient was determined as the key aging molecular phenotype module. Subsequently, the functions of the genes within the identified modules were investigated using GO and KEGG analyses.

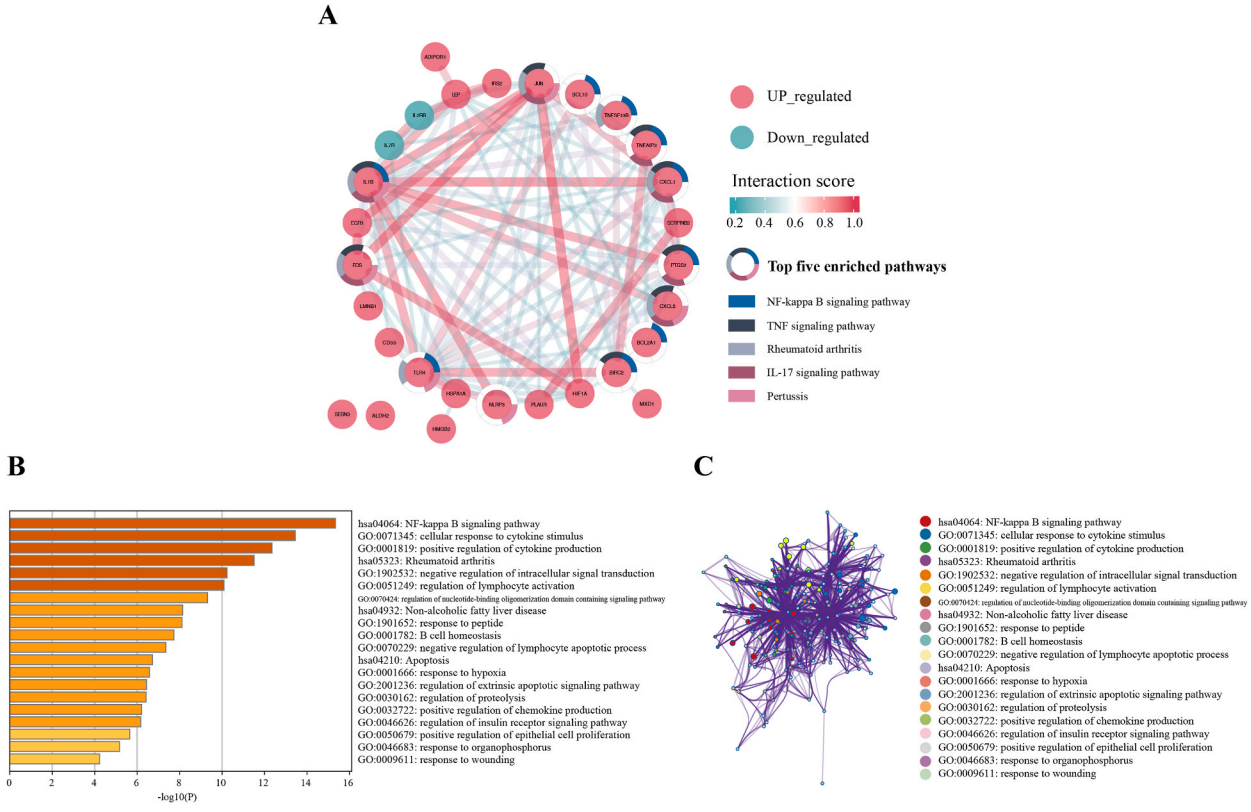

Fig. 3. Biological signatures of the 29 DE-ARGs. (A) Protein-protein interaction (PPI) network showed the proteins encoded by DE-ARGs and their relationship via the STRING database. (B) Bar graph showed the top 20 functional enrichment pathways in KEGG and GO, in which deeper color represented a lower p-value. (C) The network of the top 20 functional enrichment pathways showed the similarity of these enriched terms. Terms with a similarity score >0.3 are linked by an edge, and the thickness of the edge signifies the strength of the similarity score.

3. Results

3.1. Differentially expressed ARGs were identified in IS and control

The combination of the two datasets resulted in a unified training cohort, and the UMAP plot verified the successful batch correction(Fig. 2A and B). A total of 29 DE-ARGs were identified (Table S3), in which 27 were upregulated (*TLR4, TNFAIP3, TNFSF13B, NLRP3, FOS, CD55, HIF1A, BCL10, ALDH2, SESN3, ADIPOR1, LMNB1, LEP, CXCL5, SERPINB2, HMGB2, HSPA1A, JUN, BIRC2, PLAUR, CXCL1, IRS2, MXD1, EGR1, BCL2A1, IL1B* and *PTGS2*) and two were downregulated (*IL7R* and *IL2RB*) as shown in the volcano plot (Fig. 2C). And the PCA showed that the DE-ARGs can well distinguish the IS and control samples (Fig. 2D). Moreover, we conducted a statistical analysis (Wilcoxon rank sum test) to compare the expression levels of the differentially expressed ARGs between

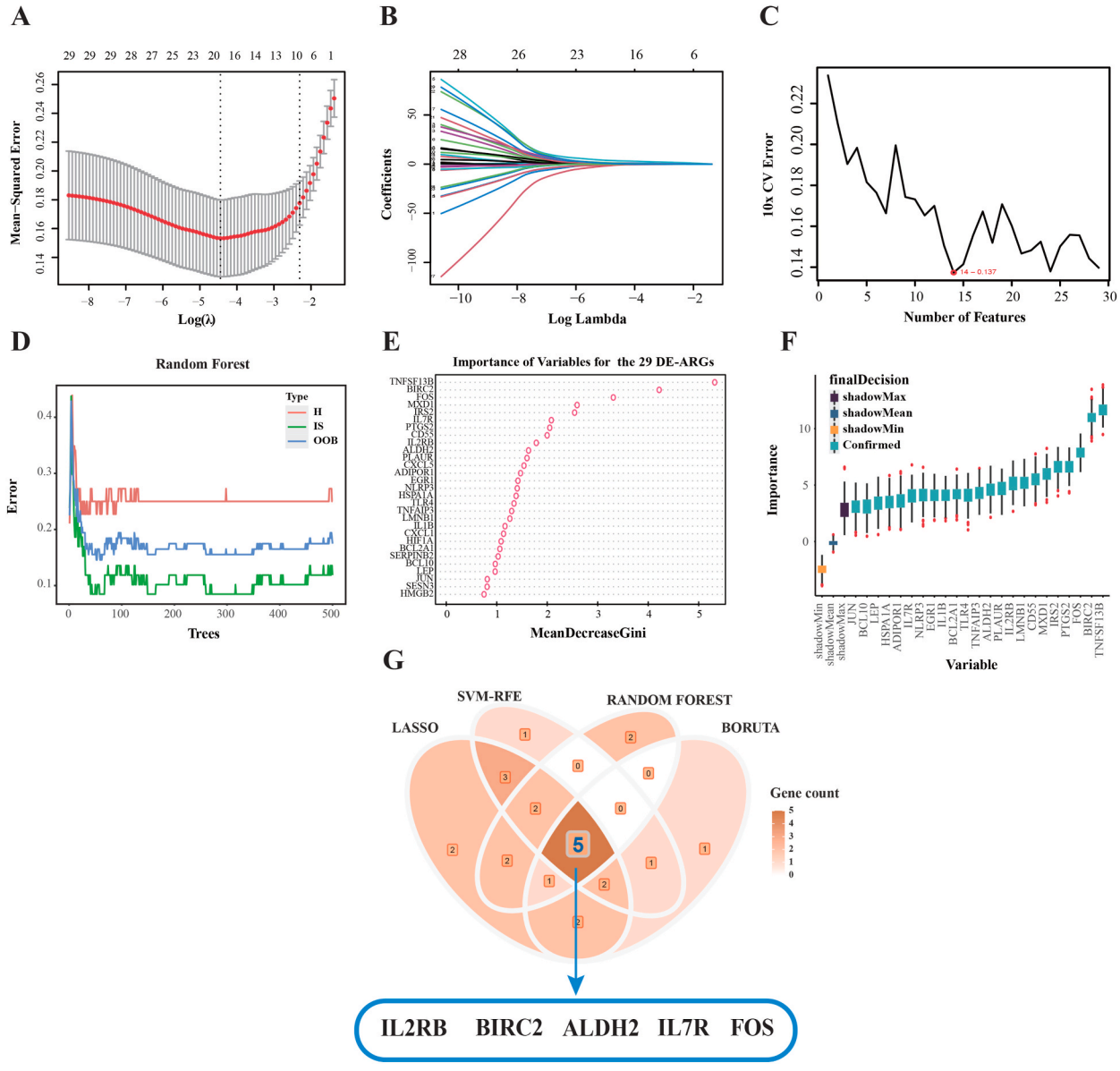

Fig. 4. Utilization of four machine learning algorithms for hub ARGs analysis. (A) The least absolute shrinkage and selection operator (LASSO) coefficient profiles of the 29 DE-ARGs. (B) LASSO was used for 10-fold cross-validation for optimum tuning parameter (l) selection. (C) Support vector machine recursive feature elimination (SVM-RFE) estimated 10-fold cross-validation error. (D) Random Forest (RF) algorithm showed the relationship between the number of decision tree and the model error. (E) RF algorithm showed the rank of importance of the 29 DE-ARGs. (F) Boruta algorithm showed the rank of importance of the 29 DE-ARGs. (G) Venn diagram showed that five hub ARGs are screened out through the four algorithms above.

the IS and control groups (Fig. 2E). Then, the DE-ARGs expression matrix was displayed by a heatmap, which showed the different expression patterns and background clinical information of gender and age between groups (Fig. 2F). At last, Spearman correlation analysis revealed the correlation between the 29 DE-ARGs, in which *TNFSF13B* and *IL7R* were the most negatively correlated pair ($r = 0.583$, $p < 2.2e\text{-}16$), while *HIF1A* and *BCL2A1* were the most positively correlated pair ($r = 0.860$, $p < 2.2e\text{-}16$) (Fig. 2G).

3.2. Inflammation-related expression patterns of the DE-ARGs were revealed

The PPI network exposed intricate connections among proteins associated with DE-ARGs (Fig. 3A), it showed that *IL1B* was strongly connected to the seven DE-ARGs, *TLR4* was related to six DE-ARGs and *JUN* was closely associated with five DE-ARGs. And *IL1B, FOS, JUN, CXCL5, PTGS2, TNFAIP3* and *TLR4* were mostly involved in the five top enriched pathways (including: NF-kappa B signaling pathway, TNF signaling pathway, Rheumatoid arthritis, IL-17 signaling pathway, and Pertussis).

A bar diagram (Fig. 3B) and corresponding network (Fig. 3C) were depicted to show the results of Metascape analysis, which both revealed the functions of DE-ARGs enriched pathways. Analysis of the histogram indicates that terms related to inflammation and immune function exhibited the highest level of enrichment, such as NF-kappa B signaling pathway, cellular response to cytokine stimulus, cytokine production, and lymphocyte activation etc.

3.3. Five hub DE-ARGs were identified through fusion of four machine learning algorithms

Four machine learning algorithms including the LASSO regression algorithm (lambda. min = 0.01173601, and 19 hub DE-ARGs were revealed in the optimization model) (Fig. 4A and B), the SVM-RFE algorithm (based on the minimum CV error, a rank of the top 14 were selected) (Fig. 4C), the RF algorithm (we set MeanDecreaseGini >1.5 as the rule out standard, and a rank of the top 12 were selected) (Fig. 4D and E), and the Boruta algorithm (a rank of the top 12/50 % were selected) (Fig. 4F) were utilized to further screen out candidate hub AGRs respectively. The candidate DE-ARGs were listed in Table S4. Finally, these candidate hub ARGs were subsequently overlapped via a Venn diagram (Fig. 4G), and five hub ARGs were identified (*IL2RB, FOS, IL7R, ALDH2* and *BIRC2*).

3.4. ANN model based on five hub DE-ARGs can predict disease status

A constructed ANN model was utilized to classify gene expression data between samples from individuals with IS and the control group, relying on the five key ARGs (Fig. 5A; Table S5). The ROC curve showed the strong dependability of our predictive model, the classifier built upon hub ARGs. It achieved an AUC of 0.951 in the training cohort and an AUC of 0.862 in the external validation cohort, indicating its high performance (Fig. 5B). Principal Component Analysis (PCA) using the five key DE-ARGs validated the effective discrimination between IS and healthy samples achieved by the ANN model (Fig. 5C). These above-mentioned results ensured the significance of the five hub DE-ARGs in IS.

3.5. Potential relationship between aging and IS: the role of immune microenvironment

As we mentioned in the introduction that neuroinflammation plays an important role in the pathogenesis of IS, which is also closely associated with aging. Correspondingly, we decided to sort out the relationship between the five hub DE-ARGs and the immune microenvironment characteristics of the IS samples, which will provide further comprehension of the underlying mechanisms. Hence immunocyte levels, immune-related pathway activities, and HLA gene expression levels were calculated and compared via Wilcoxon rank sum test between IS and control. The results showed that regulatory T cells (Tregs), plasma cells, CD8 T cells, resting dendritic

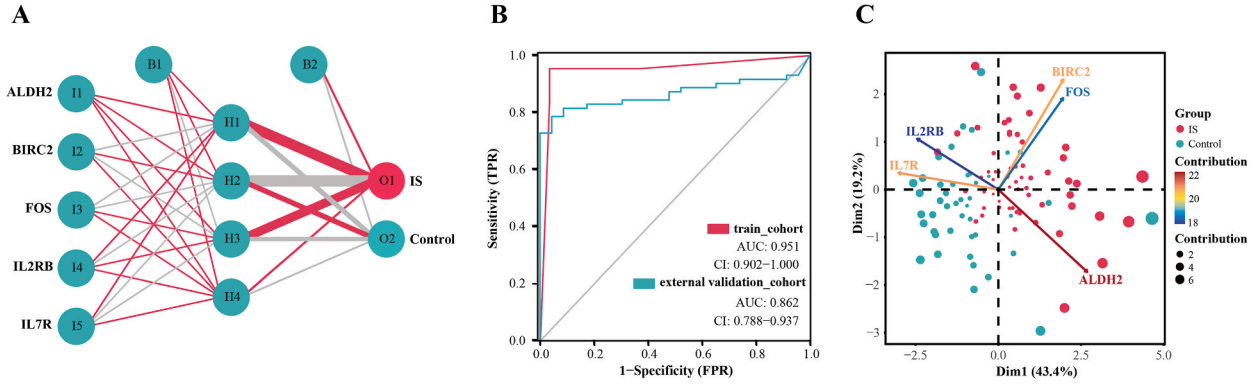

Fig. 5. Construction of artificial neural network (ANN) model. (A) ANN model has five inputs, four hidden neurons, and two outputs. In the plot, the five inputs represent the category values of the five hub DE-ARGs. (B) The ROC curve of the training cohort and external validation cohort showed reliable results of the predictive ANN model. (C) Principal component analysis (PCA) showed that the samples could be well distinguished by the five hub ARGs between IS and control, the contribution of each gene is represented by a colorful arrow.

cells, and activated NK cells were downregulated in IS, while there was an observed upregulation in gamma delta T cells, monocytes, activated mast cells, M0 macrophages and neutrophils (Fig. S3A); antigen processing and presentation, TNF family members receptors were downregulated in IS, while antimicrobials, chemokines, cytokines, interleukins receptor, TGF-beta family member and TNF family members were upregulated in IS (Fig. S3B); *HLA−DOB*, *HLA−DQA1* and *HLA−DQB1* were downregulated in IS, while *HLA−E* was upregulated (Fig. S3C).

Then, Spearman's correlation analysis was performed on the five hub DE-ARGs expression levels and the quantification outcomes of the immune microenvironment characteristics (Fig. 6B, E, H). The greatest positive and negative correlations were shown in scatter diagrams beside each correlation heatmap individually. And finally, we found that *IL2RB* correlated with monocytes the most negatively (Fig. 6A) and *ALDH2* correlated with monocytes the most positively (Fig. 6C) in the immunocyte infiltration section; *IL7R*

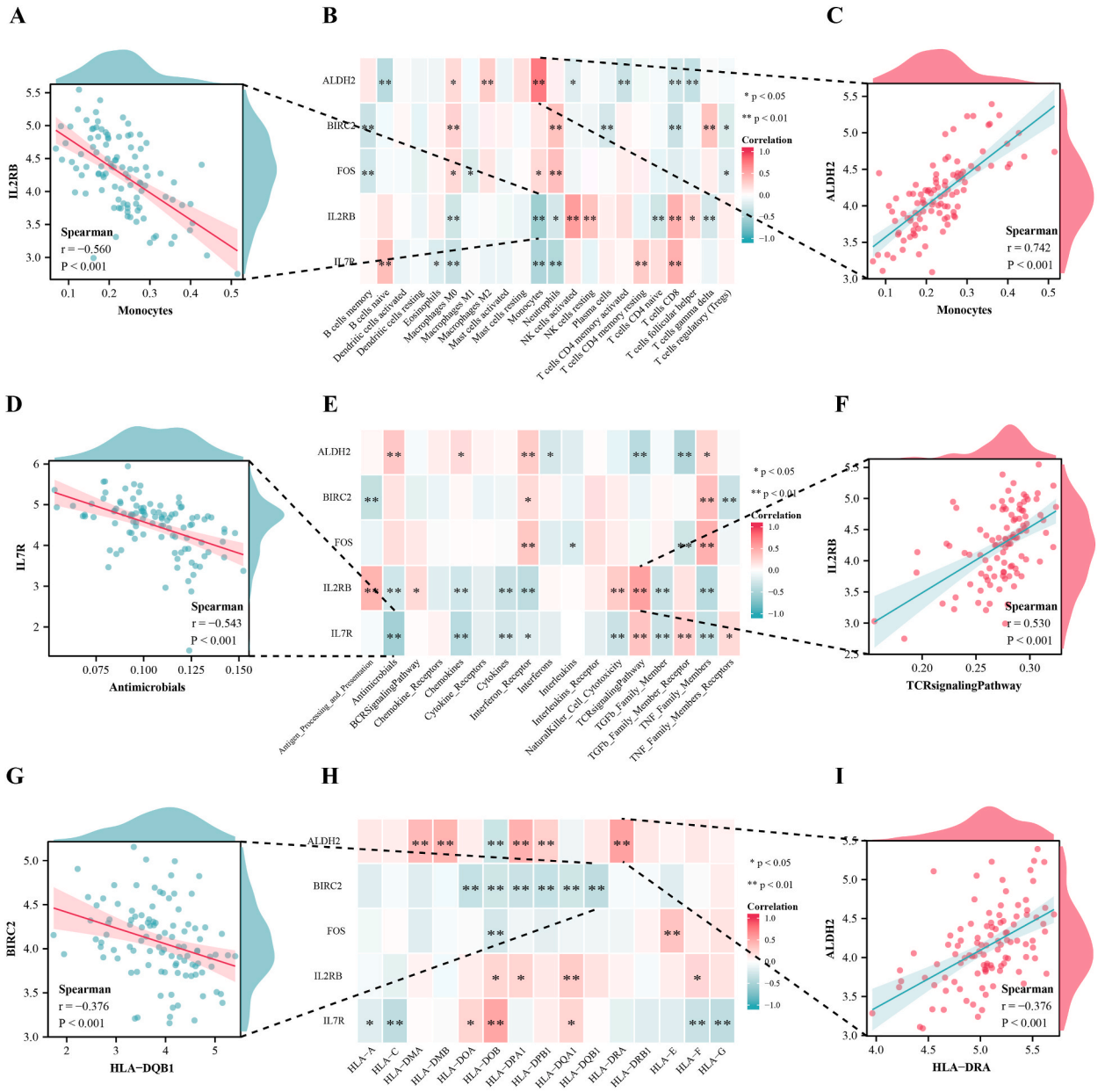

Fig. 6. Spearman correlation analyses between the five hub DE-ARGs and immune characteristics. (A) Correlation scatter plot between *IL2RB* and monocytes. (B) Correlation heatmap of the five hub DE-ARGs and the immunocyte infiltrations levels. (C) Correlation scatter plot between *ALDH2* and monocytes. (D) Correlation scatter plot between *IL7R* and antimicrobials. (E) Correlation heatmap of the five hub DE-ARGs and the enrichment scores of immune reactions. (F) Correlation scatter plot between *IL2RB* and TCR signaling pathway. (G) Correlation scatter plot between *BIRC2* and *HLA-DQB1*. (H) Correlation heatmap of the five hub DE-ARGs and the expression of HLA genes. (I) Correlation scatter plot between *ALDH2* and *HLA-DRA*. *: $P < 0.05$; **: $P < 0.01$; ns: no significance.

correlated with antimicrobials the most negatively (Fig. 6D), and *IL2RB* correlated with TCR signaling pathway the most positively (Fig. 6F) in the immune-related pathway section; and *BIRC2* correlated with *HLA-DQB1* the most negatively (Fig. 6G) and *ALDH2* correlated with *HLA−DRA* the most positively (Fig. 6I) in the HLA gene section.

3.6. *Single-cell sequencing data revealed the aging-related signature diversity in old and young mouse brains*

After quality control of the sc-seq data, low quality cells and doublets were excluded from the study (Figs. S4A–F). The basic information of each cell was exhibited (Fig. 7A), and the cells were annotated via Garnett (Fig. S5, Fig. 7B). The comparison of cell type proportions between the old and young groups revealed significant differences, particularly notable for Macrophage and Monocyte populations (Fig. 7C). Then, we exam the hub gene expression levels in old and young groups using dot plots and feature plots, and we did not find the gene Il2rb in the single-cell data, which may be due to the distinct sequencing protocol, and we found that hub gene

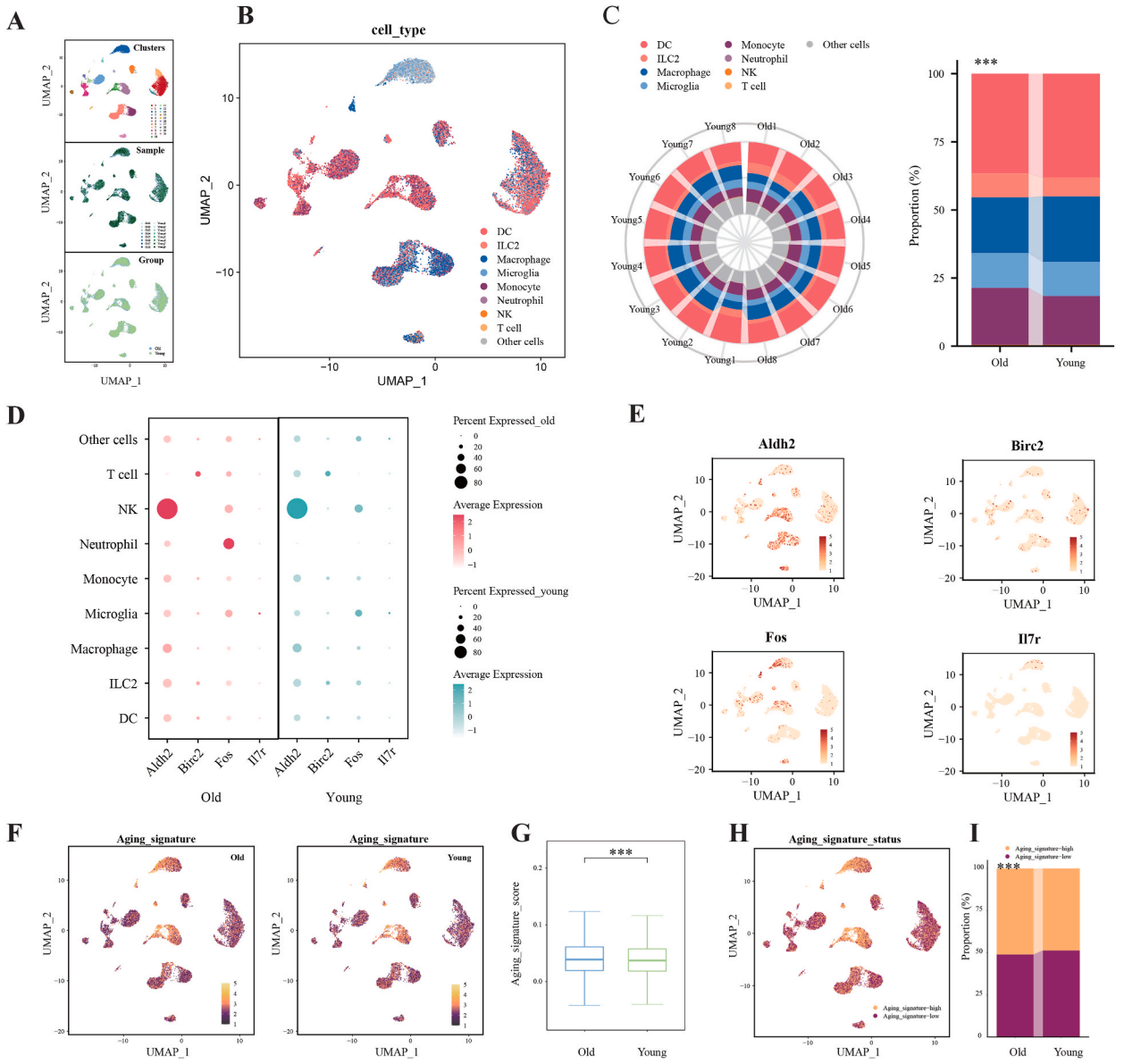

Fig. 7. Aging characteristics on single-cell sequencing resolution. (A) UMAP representation of basic information. (B) UMAP representation of major cell types based on canonical markers and signature-based annotation using Garnett. (C) Proportion plots of major cell types in old and young samples and groups. (D) Dotplot showed the expression levels of four hub genes in each cell type. (E) Feature plot showed the expression levels of four hub genes. (F) Feature plots showed the aging signature in old and young groups. (G) Boxplot showed the aging signature difference in old and young groups. (H) Feature plot marked the aging signature status in each cell. (H) Proportion plots of aging signature status in old and young groups.

Aldh2 was mainly expressed in natural killer (NK) cells and the expression levels of Fos in Neutrophils were obviously elevated in the aged mouse brain (Fig. 7D and E). Subsequently, the aging signatures were evaluated (Fig. 7F), and our investigation indicated a notable increase in aging signature scores among individuals in the old group compared to those in the young group (Fig. 7G). We next assessed the aging signature status in every cell (Fig. 7H) and found that the clinical old group had a significantly bigger proportion of aging signature−high cells (Fig. 7I).

3.7. Detection of two distinct molecular subtypes associated with aging in IS

The unsupervised consistent cluster analysis identified two distinct aging-related molecular subtypes in IS **(Supplementary Figs. 6A–D)**, which is reliant on expression levels of the differentially expressed key ARGs. Besides, the PCA diagram confirmed that subtype 1 and subtype 2 could be well distinguished by the clustering method (Fig. 8A). And the Wilcoxon rank sum test showed that *BCL10, BCL2A1, CXCL1, IL1B, JUN, NLRP3, PLAUR, PTGS2, SERPINB2* and *TNFAIP3* were upregulated in subtype 2, and *FOS, HSPA1A* and *TNFSF13B* were upregulated in subtype 1 (Fig. 8B). In addition, the functional enrichment pathways and immune characteristics of the subtypes were examined. Through the HALLMARKS pathway bar diagram, we found that NF-kappa B-regulated TNF-a signaling pathway and spermatogenesis activity were highly enriched in subtype 2, meanwhile, protein secretion activity and reactive oxygen species pathway were highly enriched in subtype 1 (Fig. 8C). And through the heatmap of the Reactome pathway, we confirmed that the enrichment patterns were quite different between subtypes (Fig. 8D**)**.

And the supplementary Wilcoxon rank sum test showed that memory B cells, follicular helper T cells, and activated mast cells were upregulated in subtype 2; and CD4 naive T cells, monocytes, M0 macrophages and neutrophils were upregulated in subtype 1 (Fig. 9A); antigen processing and presentation, chemokines, cytokines and interleukins were upregulated in subtype 2, and chemokine receptors, interferon receptors, and TNF family members were upregulated in subtype 1 (Fig. 9B); In subtype 2, the expression levels of *HLA-DOB* and *HLA-DRA* were found to be elevated, while no upregulation of HLA genes was observed in subtype 1 (Fig. 9C).

3.8. Biological characteristics of aging-related molecular subtypes

To gain deeper insights into the molecular mechanisms underlying genes' involvement in aging-related regulations, DEGs between subtype 1 and subtype 2 were screened out (Fig. 10A) and subjected to WGCNA to locate aging molecular phenotype-related genes, and the greenyellow module was determined as the key module due to the most significant p-value and the highest correlation coefficients (Fig. 10B, Table S6). Following that, GO and KEGG pathway analyses were conducted to delve into the potential mechanisms associated with the greenyellow gene network module related to aging. In biological process (BP) enrichment analysis, genes in

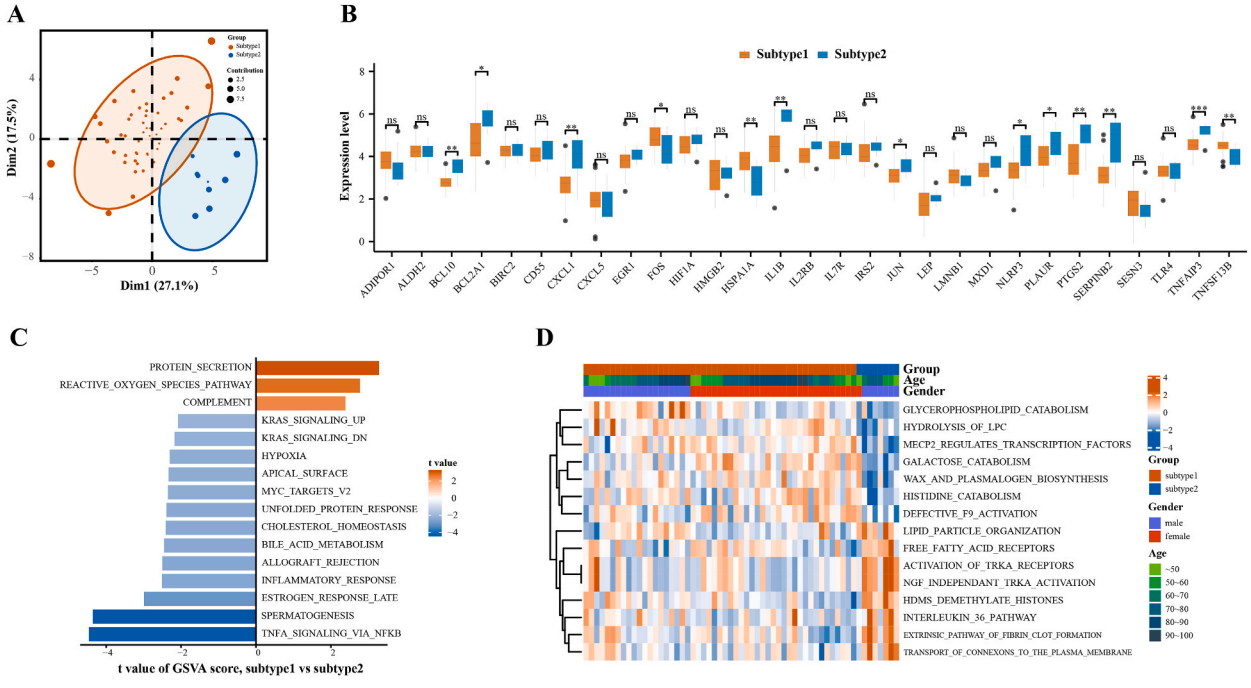

Fig. 8. Unsupervised clustering of the 29 DE-ARGs identified two distinct aging-related subtypes in IS cases. (A) PCA showed a remarkable difference in transcriptome profiles between the two subtypes. (B) Wilcoxon rank sum test compared the expression levels of the 29 DE-ARGs in the two subtypes (Data are expressed as means ± SD, *: P < 0.05; **: P < 0.01; ***: P < 0.001; ns: no significance). (C, D) The underlying biological function characteristics diversity between the distinct subtypes, and the differences of the HALLMARKS pathway and Reactome pathway enrichment score between subtype-1 and subtype-2 (C for the HALLMARKS pathway and D for the Reactome pathway).

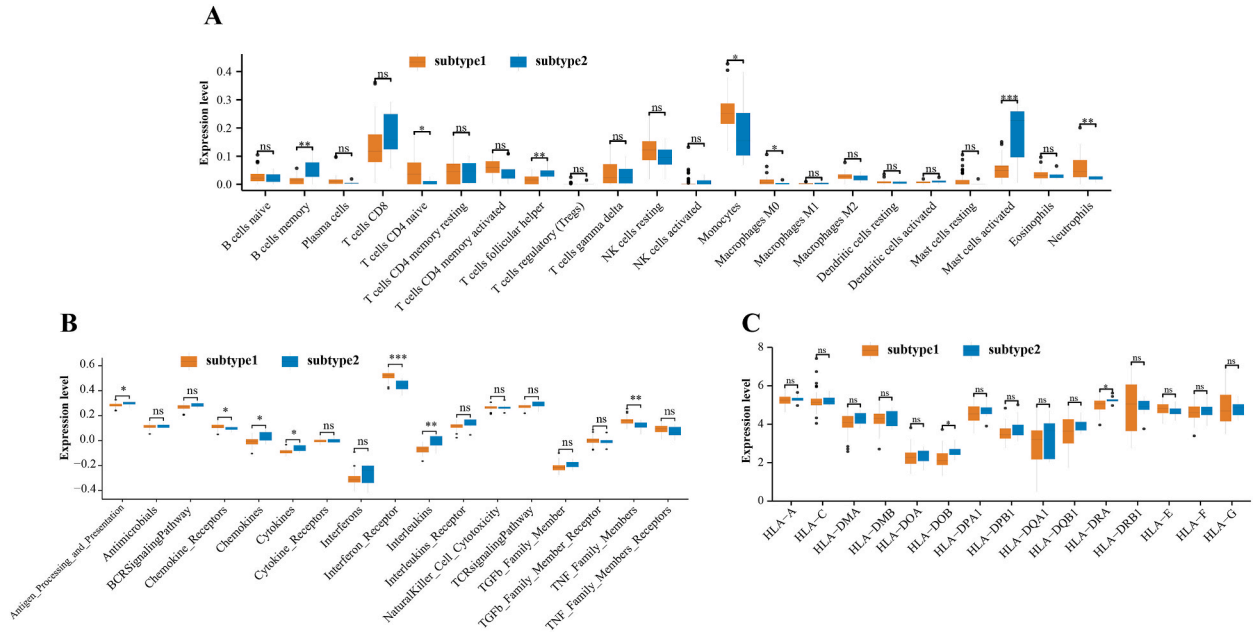

Fig. 9. Wilcoxon rank sum test of the immune characteristics between the two subtypes. (A) Wilcoxon rank sum test compared the immunocyte levels; (B) the immune-related pathway activities; and (C) the HLA gene expression levels between the two subtypes. Data are expressed as means ± SD, *: P < 0.05; **: P < 0.01; ***: P < 0.001; ns: no significance.

greenyellow module were found to be mostly enriched in nuclear-related transport activities such as RNA, DNA and protein import to or export from nuclear. In cellular component (CC) enrichment analysis, genes were found to be involved in nuclear pore, chaperone complex, nuclear envelope, SWI/SNF superfamily-type complex and ATPase complex. And in molecular function (MF) enrichment analysis, genes were found to be involved in chaperone binding and misfolded protein binding (Fig. 10C). The top ten KEGG pathways were shown in the cyclograph (Fig. 10D), which suggest that the greenyellow module genes exhibited significant enrichment in RNA transport, T-cell receptor signaling pathway, ribosome biogenesis in eukaryotes, Th17 cell differentiation, and human T-cell leukemia virus 1 infection et al.

4. Discussion

Immune-related neuroinflammation plays a vital role in IS evolution, and immunosenescence has been identified as a potential contributor to age-related brain injury and neurodegenerative diseases as poorer outcomes have been observed in IS due to aging-originated alterations in the immune system of the elderly [15]. However, there were no existing microarray or single cell datasets originated from IS patients' brains, which would be the most convincing in gene function analyses. Fortunately, immunosenescence is a process which can also be measured by blood [13] so that we acquired all the high-quality microarray datasets of human blood samples from GEO database to find out the potential effect of the ARGs in IS. The current investigation utilized diverse bioinformatics analyses to detect regulators associated with aging in IS and unveil ARG signatures. The expression and regulation of the ARGs are influenced by aging. Revealing their biological functions may contribute to a better comprehension of the ARGs in IS pathogenesis. In summary, we identified 29 ARGs closely associated with IS, which informed us of the potential mechanisms of how aging influence IS progression and outcomes.

From the functional enrichment analyses, these DE-ARGs were found to be significantly involved in NF-kappa B signaling pathway. And NF-kappa B transcription factors are critical regulators of the development of innate and adaptive immunity [50]. As a consequence of all NF-kappa B proteins sharing a Rel homology domain responsible for DNA binding and dimerization, dysregulation of NF-kappa B activity is linked to autoimmune diseases, inflammatory and metabolic disorders, as well as cancer [51–53]. Indeed, NF-kappa B signaling pathway has been reported as a key regulator in IS progression and treatment recently [54–56]. In our study, the DE-ARGs which participated in the NF-kappa B signaling pathway (*BCL10, TNFSF13B, TNFSAIP3, CXCL1, PTGS2, BCL2A1, BIRC2, IL1B and TLR4*) were found all upregulated in IS. Therefore, our results combined with these above-mentioned findings may indicate that aging may influence our immune functions via over-activating the NF-kappa B signaling pathway or at least related to the dysfunction of it, and thus more likely to cause excess neuroinflammation in elder IS patients.

Meanwhile, these DE-ARGs were also involved in cytokine activities such as cellular response to cytokine stimulus and positive regulation of cytokine production, as well as IL-17 signaling pathway and TNF signaling pathway. Noteworthy, previous studies have demonstrated that many cytokines play vital roles in IS, such as interleukins [57,58], tumor necrosis factor-alpha [59,60], transforming growth factor-beta [61], granulocyte colony stimulating factor [62] and erythropoietin [63]. The results may indicate that

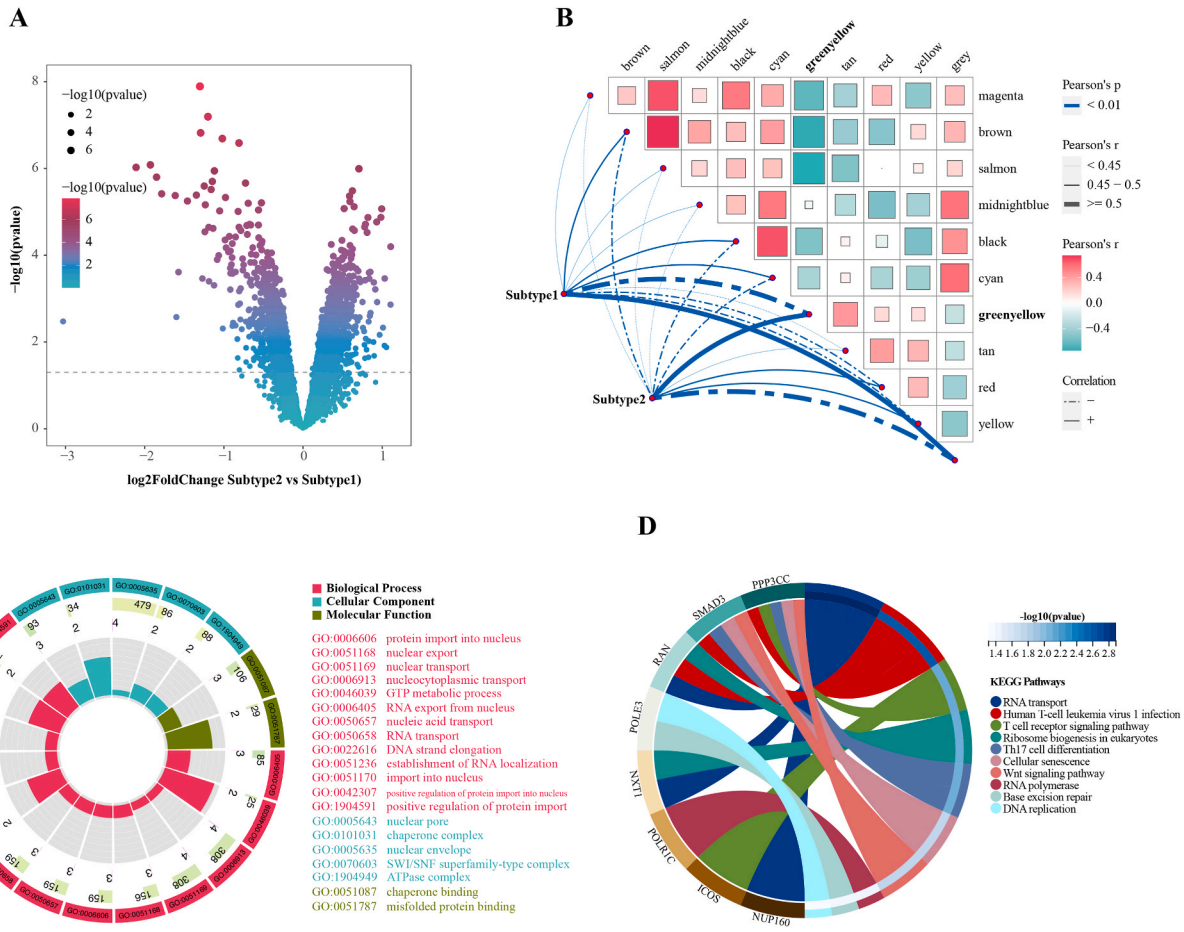

Fig. 10. Co-expression networks and biological signatures of the DEGs between subtypes. (A) DEGs were identified between subtype 1 and subtype 2. (B) Correlation heatmap showed the relationship between module eigengenes and the two aging-related subtypes. (C) GO enrichment analysis of aging phenotype-related genes in greenyellow module. The outermost ring displayed the ID of pathways, the second outer ring showed the number of genes in pathways, and the heights of the columns in the inner ring indicated the value of GeneRatio. (D) Chord plot depicted the relationship between greenyellow module genes and KEGG signaling pathways.

aging may alter cytokine activities and hence influence the outcome of IS. Besides, some other pathways were already thought to be important in IS progression, such as apoptosis and response to hypoxia [64,65]. As poorer outcomes have been observed in elder patients of IS, we assume that aging may potentially augment the sensitivity of cellular response to hypoxia and contribute to the apoptotic process.

By applying four machine learning algorithms, five hub ARGs were identified (*IL2RB, FOS, IL7R, ALDH2, BIRC2*), in which *ALDH2, BIRC2* and *FOS* were upregulated in IS, and *IL2RB, IL7R* were downregulated. As previously reported, *IL2RB* is primarily expressed in the hematopoietic system and encodes the interleukin 2 receptor, which serves as a crucial mediator in regulating the immune response by integrating signals derived from the pivotal cytokines IL-2 and IL-15; *IL2RB* mutation or deficiency can lead to immunodeficiency and autoimmunity [66]. *ALDH2* is an important detoxification enzyme with a potent effect on ethanol metabolism, and it also shields our inner microenvironment from oxidative stress [67,68]. Evidence from an experimental study has also suggested that *ALDH2* conferred neuroprotection on cerebral ischemic injury and reduced the size of cerebral infarct [69]. Contrarily, population-based investigations have demonstrated a strong correlation between *ALDH2* genetic polymorphism and the rising prevalence of cardiovascular risk factors and stroke occurrences [70,71].

The Fos gene family comprises four distinct members, namely *FOS, FOSB, FOSL1*, and *FOSL2*. These genes are responsible for encoding leucine zipper proteins that have the ability to form a transcription factor complex known as AP-1 by dimerizing with proteins from the JUN family. Consequently, the Fos proteins have been implicated in the regulation of various cellular processes such as proliferation, differentiation, and transformation (source: https://www.ncbi.nlm.nih.gov/gene/2353). Previous research has provided evidence indicating the significance of Fos as a crucial connection between hypertension and IS, indicating the possibility of utilizing it as a prospective target for stroke prevention and treatment in hypertensive patients by inhibiting apoptosis and oxidative stress after onset [72]. And Fos downstream transcript is a functionally promising target to protect IS patients from ischemic brain damage and facilitate neurological recovery [73].

IL7R is responsible for encoding a protein receptor that specifically interacts with interleukin 7 (IL-7), which has been demonstrated to have a vital involvement in the development of lymphocytes [74]. Abnormalities in this gene could potentially be linked to a condition known as severe combined immunodeficiency, characterized by compromised immune function [75]. *BIRC2* encoded proteins that inhibit apoptosis by binding to tumor necrosis factor receptor-associated factors TRAF1 and TRAF2, especially the apoptosis induced by serum deprivation and menadione, a potent inducer of free radicals (https://www.ncbi.nlm.nih.gov/gene/329). It may inform us that *BICR2* may be related to IS through apoptosis, but few studies have been reported, hence, how *BICR2* plays its part in the apoptosis process in IS requires further investigations.

Owing to all above, *BIRC2* and *FOS* can inhibit apoptosis; *IL2RB* and *IL7R* are more related to immune functions, deficiency or mutation of the genes can lead to immunodeficiency; *ALDH2* encodes detoxification enzyme with potent effect in ethanol metabolism, and shield our inner microenvironment from oxidative stress. It has been indicated in the results that *ALDH2*, *BIRC2* and *FOS* were upregulated in IS, and *IL2RB, IL7R* were downregulated. Therefore, we conclude that the upregulated hub DE-ARGs may present protective effects after IS onset, which may be a compensatory mechanism. And the downregulated hub genes may contribute to detrimental aging-related immune dysregulation and overcome the protective effects, thus leading to adverse outcomes in IS. In addition, other DE-ARGs were also noticed in immune functions, for instance, *HIF1A* and *JUN* have been reported to be the key immunosuppression-related crosstalk genes in stroke [76]. The upregulation of these two genes in this study may collaborate with *IL2RB* and *IL7R*, thus contributing to immune dysregulation in IS. These results may provide new insights into how aging influence IS development, and further investigations are in demand.

Next, by comparing the immune characteristics between IS and control, the quantification results of most immune cells, enriched immune pathways and HLA genes were elevated in IS, suggesting significant differences in the immune microenvironment of IS and control. Besides, Spearman's correlation analysis revealed a strong relationship between immune microenvironment characteristics and DE-ARGs, especially highlighted with *ALDH2* and *IL2RB*. The findings suggest a significant association between the immune system and the progression of IS, which is further influenced by the aging process. Next, mouse brain single-cell sequencing data also revealed age-related signature diversity emphasized with the proportion of cell types, which were significantly different between the old and young mouse brains. Overall, the proportion of monocytes was increased in the old group while the proportion of macrophage was decreased. Furthermore, the bubble plot showed the expression of *Aldh2* on the NK cell was increased in the old group, and *Fos* was mostly expressed on neutrophil in the old group instead of the young group, which was in accordance with the expression results analyzed from peripheral blood microarray datasets. Subsequently, we utilized the ARGs to calculated the aging signature scores for each cell, which revealed that the old group had significantly higher aging signature scores and had a significantly bigger proportion of aging signature−high cells than the young group. Previous studies have discussed post-stroke immune cell heterogeneity in the brain and uncovered distinct functional immune subpopulations in stroke pathophysiology [45]. Similarly in this study, both in CNS and peripheral immune system showed potential effects of aging on immune system, these results may indicate that aging largely determines immune function and may thus influence IS outcome, future studies are highly recommended in investigating these findings by experimental methods.

To gain deeper insights into the mechanistic aspects of IS, unsupervised consistent cluster analysis was employed, leading to the identification of two discrete aging-related molecular IS subtypes. This highlights the strong influence of aging on the IS immune microenvironment. The GSVA results indicated that subtype 2 was enriched in NF-kappa B-regulated TNF-a signaling pathway and spermatogenesis activity, whereas subtype 1 was involved in protein secretion activity and reactive oxygen species pathway. And the WGCNA results confirmed the differences between groups. In conclusion, these results indicated that IS cases may have two clusters characterized by different mechanisms. And the enriched NF-kappa B regulated TNF-a signaling pathway in subtype 2 also strengthened the conclusion that aging may influence our immune microenvironment and immune functions via upregulating the NF-kappa B signaling pathway, and thus more likely to cause excess neuroinflammation in elder IS patients. Additionally, a recent study concerning prostate cancer demonstrated that activation of *IL2RB* can inhibit the NF-kappa B signaling pathway [77], and it is worth noting that the NF-kappa B signaling pathway has been identified as a critical therapeutic target in IS neuroinflammation [78,79], which showed the DE-ARGs may participate in the development and progression of IS in subtle ways but need to be studied furtherly.

5. Conclusions

In the present study, we identified 29 ARGs closely related to IS. And the DE-ARGs that were significantly involved in the NF-kappa B signaling pathway were all upregulated in IS, which indicated that aging may cause excess neuroinflammation in elder IS patients via upregulating the NF-kappa B signaling pathway. Next, five hub ARGs were identified (*IL2RB, FOS, IL7R, ALDH2, BIRC2*) by overlapping four machine learning algorithms, which were believed to contribute to immune dysregulation in IS and thus lead to adverse outcomes. At last, two distinct aging-related molecular IS subtypes were identified, and the following GSVA and WGCNA results provide supporting evidence for the substantial involvement of the NF-kappa B signaling pathway in immune homeostasis regulation of IS development. These results may provide new insights into how aging influence IS development and reveal potential therapeutic targets. Nevertheless, it is essential to acknowledge that this study is based on in silico analysis, and while the findings are theoretically sound, they have not yet been experimentally validated. While the use of an external validation dataset in the present study can serve as a viable alternative to experimental validation to some extent, we suggest that experimental validation would be a more robust approach. Besides, regarding a possible sex effect in the data, we did account for it in our analysis but did not investigate any potential sex-specific effects due to the limited sample size, future investigations will explore this issue.

Author contribution statement

Zhengyu Yao: Conceived and designed the experiments; Performed the experiments; Analyzed and interpreted the data; Contributed reagents, materials, analysis tools or data; Wrote the paper.

Jin Jiang: Analyzed and interpreted the data.

Yaxin Ju: Contributed reagents, materials, analysis tools or data.

Yong Luo: Conceived and designed the experiments; Wrote the paper.

Data availability statement

Data associated with this study has been deposited at Gene Expression Omnibus (GEO) database (https://www.ncbi.nlm.nih.gov/geo/); Accession number: GSE22255, GSE16561, GSE58294 and GSE129788.

Declaration of competing interest

The authors declare that they have no known competing financial interests or personal relationships that could have appeared to influence the work reported in this paper.

Acknowledgments

This study was funded by the National Natural Science Foundation of China (Grant No. 30470606), the Postdoctoral Training ProgramFoundation of the First Affiliated Hospital of Chongqing Medical University (Grand NO. CYYY-BSHPYXM-202214) and the China Postdoctoral Science Foundation (Grand NO. 2022MD723736).

Appendix A. Supplementary data

Supplementary data to this article can be found online at https://doi.org/10.1016/j.heliyon.2023.e21071.

References

[1] F. Herpich, F. Rincon, Management of acute ischemic stroke, Crit. Care Med. 48 (11) (2020) 1654–1663.
[2] V.A. Pavlov, S.S. Chavan, K.J. Tracey, Molecular and functional neuroscience in immunity, Annu. Rev. Immunol. 36 (2018) 783–812.
[3] M. Prinz, J. Priller, The role of peripheral immune cells in the CNS in steady state and disease, Nat. Neurosci. 20 (2) (2017) 136–144.
[4] I.J. Elenkov, et al., The sympathetic nerve–an integrative interface between two supersystems: the brain and the immune system, Pharmacol. Rev. 52 (4) (2000) 595–638.
[5] M.J. Kenney, C.K. Ganta, Autonomic nervous system and immune system interactions, Compr. Physiol. 4 (3) (2014) 1177–1200.
[6] R.L. Jayaraj, et al., Neuroinflammation: friend and foe for ischemic stroke, J. Neuroinflammation 16 (1) (2019) 142.
[7] E.B. Engler-Chiurazzi, et al., Role of B cells and the aging brain in stroke recovery and treatment, Geroscience 42 (5) (2020) 1199–1216.
[8] K. Mayne, et al., Aging and neurodegenerative disease: is the adaptive immune system a friend or foe? Front. Aging Neurosci. 12 (2020), 572090.
[9] M. Roy-O'Reilly, L.D. McCullough, Age and sex are critical factors in ischemic stroke pathology, Endocrinology 159 (8) (2018) 3120–3131.
[10] G. Saposnik, et al., Stroke outcome in those over 80: a multicenter cohort study across Canada, Stroke 39 (8) (2008) 2310–2317.
[11] B.A. Drozdowska, S. Singh, T.J. Quinn, Thinking about the future: a review of prognostic scales used in acute stroke, Front. Neurol. 10 (2019) 274.
[12] L.E. Heitsch, P.D. Panagos, Treating the elderly stroke patient: complications, controversies, and best care metrics, Clin. Geriatr. Med. 29 (1) (2013) 231–255.
[13] M.J. Yousefzadeh, et al., An aged immune system drives senescence and ageing of solid organs, Nature 594 (7861) (2021) 100–105.
[14] R.M. Ritzel, et al., Aging alters the immunological response to ischemic stroke, Acta Neuropathol. 136 (1) (2018) 89–110.
[15] C. Iadecola, M.S. Buckwalter, J. Anrather, Immune responses to stroke: mechanisms, modulation, and therapeutic potential, J. Clin. Invest. 130 (6) (2020) 2777–2788.
[16] A. Lasry, Y. Ben-Neriah, Senescence-associated inflammatory responses: aging and cancer perspectives, Trends Immunol. 36 (4) (2015) 217–228.
[17] L. Peng, et al., Identification and validation of a classifier based on hub aging-related genes and aging subtypes correlation with immune microenvironment for periodontitis, Front. Immunol. 13 (2022), 1042484.
[18] J. He, X. Li, Identification and validation of aging-related genes in idiopathic pulmonary fibrosis, Front. Genet. 13 (2022), 780010.
[19] Q. Zhang, J. Li, L. Weng, Identification and validation of aging-related genes in alzheimer's disease, Front. Neurosci. 16 (2022), 905722.
[20] T. Zeng, et al., The establishment of a prognostic scoring model based on the new tumor immune microenvironment classification in acute myeloid leukemia, BMC Med. 19 (1) (2021) 176.
[21] T. Krug, et al., TTC7B emerges as a novel risk factor for ischemic stroke through the convergence of several genome-wide approaches, J. Cerebr. Blood Flow Metabol. 32 (6) (2012) 1061–1072.
[22] T.L. Barr, et al., Genomic biomarkers and cellular pathways of ischemic stroke by RNA gene expression profiling, Neurology 75 (11) (2010) 1009–1014.
[23] J. Taminau, et al., Unlocking the potential of publicly available microarray data using inSilicoDb and inSilicoMerging R/Bioconductor packages, BMC Bioinf. 13 (1) (2012) 335.
[24] C. Chen, et al., Removing batch effects in analysis of expression microarray data: an evaluation of six batch adjustment methods, PLoS One 6 (2) (2011), e17238.
[25] B. Stamova, et al., Gene expression in peripheral immune cells following cardioembolic stroke is sexually dimorphic, PLoS One 9 (7) (2014), e102550.
[26] A.A. Consortium, Aging Atlas: a multi-omics database for aging biology, Nucleic Acids Res. 49 (D1) (2021) D825–d830.
[27] R. Tacutu, et al., Human ageing genomic resources: new and updated databases, Nucleic Acids Res. 46 (D1) (2018) D1083–d1090.
[28] M.E. Ritchie, et al., Limma powers differential expression analyses for RNA-sequencing and microarray studies, Nucleic Acids Res. 43 (7) (2015) e47.
[29] P. Shannon, et al., Cytoscape: a software environment for integrated models of biomolecular interaction networks, Genome Res. 13 (11) (2003) 2498–2504.
[30] D. Szklarczyk, et al., STRING v10: protein-protein interaction networks, integrated over the tree of life, Nucleic Acids Res. 43 (Database issue) (2015) D447–D452.

[31] J. Friedman, T. Hastie, R. Tibshirani, Sparse inverse covariance estimation with the graphical lasso, Biostatistics 9 (3) (2008) 432–441.
[32] H. Sanz, et al., SVM-RFE: selection and visualization of the most relevant features through non-linear kernels, BMC Bioinf. 19 (1) (2018) 432.
[33] M.B. Kursa, W.R. Rudnicki, Feature selection with the Boruta package, J. Stat. Software 36 (11) (2010) 1–13.
[34] K.C. Yuan, et al., The development an artificial intelligence algorithm for early sepsis diagnosis in the intensive care unit, Int J Med Inform 141 (2020), 104176.
[35] S. RcolorBrewer, M.A.J.U.o.C. Liaw, Berkeley: Berkeley, CA, USA, Package 'randomforest', 2018.
[36] P. Charoentong, et al., Pan-cancer immunogenomic analyses reveal genotype-immunophenotype relationships and predictors of response to checkpoint blockade, Cell Rep. 18 (1) (2017) 248–262.
[37] S. Bhattacharya, et al., ImmPort: disseminating data to the public for the future of immunology, Immunol. Res. 58 (2–3) (2014) 234–239.
[38] M. Ximerakis, et al., Single-cell transcriptomic profiling of the aging mouse brain, Nat. Neurosci. 22 (10) (2019) 1696–1708.
[39] Y. Hao, et al., Integrated analysis of multimodal single-cell data, Cell 184 (13) (2021) 3573–3587.e29.
[40] Z. Wang, et al., DNER and GNL2 are differentially m6A methylated in periodontitis in comparison with periodontal health revealed by m6A microarray of human gingival tissue and transcriptomic analysis, J. Periodontal. Res. 58 (3) (2023) 529–543.
[41] C.S. McGinnis, L.M. Murrow, Z.J. Gartner, DoubletFinder: doublet detection in single-cell RNA sequencing data using artificial nearest neighbors, Cell Syst 8 (4) (2019) 329–337.e4.
[42] I. Tirosh, et al., Dissecting the multicellular ecosystem of metastatic melanoma by single-cell RNA-seq, Science 352 (6282) (2016) 189–196.
[43] I. Korsunsky, et al., Fast, sensitive and accurate integration of single-cell data with Harmony, Nat. Methods 16 (12) (2019) 1289–1296.
[44] H.A. Pliner, J. Shendure, C. Trapnell, Supervised classification enables rapid annotation of cell atlases, Nat. Methods 16 (10) (2019) 983–986.
[45] X. Li, et al., Single-cell transcriptomic analysis of the immune cell landscape in the aged mouse brain after ischemic stroke, J. Neuroinflammation 19 (1) (2022) 83.
[46] S. Jiang, et al., Cell Taxonomy: a curated repository of cell types with multifaceted characterization, Nucleic Acids Res. 51 (D1) (2023) D853–d860.
[47] L. Bullinger, et al., Use of gene-expression profiling to identify prognostic subclasses in adult acute myeloid leukemia, N. Engl. J. Med. 350 (16) (2004) 1605–1616.
[48] M.D. Wilkerson, D.N. Hayes, ConsensusClusterPlus: a class discovery tool with confidence assessments and item tracking, Bioinformatics 26 (12) (2010) 1572–1573.
[49] S. Hänzelmann, R. Castelo, J. Guinney, GSVA: gene set variation analysis for microarray and RNA-seq data, BMC Bioinf. 14 (2013) 7.
[50] A. Oeckinghaus, M.S. Hayden, S. Ghosh, Crosstalk in NF-κB signaling pathways, Nat. Immunol. 12 (8) (2011) 695–708.
[51] A. Kumar, et al., Nuclear factor-kappaB: its role in health and disease, J. Mol. Med. (Berl.) 82 (7) (2004) 434–448.
[52] R.G. Baker, M.S. Hayden, S. Ghosh, NF-κB, inflammation, and metabolic disease, Cell Metab 13 (1) (2011) 11–22.
[53] M. Karin, Nuclear factor-kappaB in cancer development and progression, Nature 441 (7092) (2006) 431–436.
[54] Q. Xia, et al., TRIM45 causes neuronal damage by aggravating microglia-mediated neuroinflammation upon cerebral ischemia and reperfusion injury, Exp. Mol. Med. 54 (2) (2022) 180–193.
[55] Q. Xu, et al., Relevant mediators involved in and therapies targeting the inflammatory response induced by activation of the NLRP3 inflammasome in ischemic stroke, J. Neuroinflammation 18 (1) (2021) 123.
[56] M. Liu, et al., Cottonseed oil alleviates ischemic stroke injury by inhibiting the inflammatory activation of microglia and astrocyte, J. Neuroinflammation 17 (1) (2020) 270.
[57] P. Kumar, et al., Role of Interleukin-10 (-1082A/G) gene polymorphism with the risk of ischemic stroke: a meta-analysis, Neurol. Res. 38 (9) (2016) 823–830.
[58] D. Chen, et al., Interleukin 13 promotes long-term recovery after ischemic stroke by inhibiting the activation of STAT3, J. Neuroinflammation 19 (1) (2022) 112.
[59] J.C. Wu, et al., Gene polymorphisms and circulating levels of the TNF-alpha are associated with ischemic stroke: a meta-analysis based on 19,873 individuals, Int Immunopharmacol 75 (2019), 105827.
[60] P. Kumar, et al., Association between tumor necrosis factor-α (-238G/A and -308G/A) gene polymorphisms and risk of ischemic stroke: a meta-analysis, Pulse (Basel) 3 (3–4) (2016) 217–228.
[61] P. Kumar, et al., Association of transforming growth factor beta-1-509C/T gene polymorphism with ischemic stroke: a meta analysis, Basic Clin. Neurosci. 7 (2) (2016) 91–96.
[62] X. Huang, et al., Granulocyte colony stimulating factor therapy for stroke: a pairwise meta-analysis of randomized controlled trial, PLoS One 12 (4) (2017), e0175774.
[63] M. Digicaylioglu, Erythropoietin in stroke: quo vadis, Expert Opin Biol Ther 10 (6) (2010) 937–949.
[64] T.I. Nathaniel, et al., Tissue hypoxia during ischemic stroke: adaptive clues from hypoxia-tolerant animal models, Brain Res. Bull. 114 (2015) 1–12.
[65] J. Yao, et al., Hypoxia related long non-coding RNAs in ischemic stroke, Noncoding RNA Res 6 (4) (2021) 153–158.
[66] Z. Zhang, et al., Human interleukin-2 receptor β mutations associated with defects in immunity and peripheral tolerance, J. Exp. Med. 216 (6) (2019) 1311–1327.
[67] Y.C. Chao, et al., Polymorphism of alcohol and aldehyde dehydrogenase genes and alcoholic cirrhosis in Chinese patients, Hepatology 19 (2) (1994) 360–366.
[68] W. Tian, et al., The discovery of novel small molecule allosteric activators of aldehyde dehydrogenase 2, Eur. J. Med. Chem. 212 (2021), 113119.
[69] P. Xia, et al., ALDH 2 conferred neuroprotection on cerebral ischemic injury by alleviating mitochondria-related apoptosis through JNK/caspase-3 signing pathway, Int. J. Biol. Sci. 16 (8) (2020) 1303–1323.
[70] X. Cheng, et al., Genetic variants in ALDH2 predict risk of ischemic stroke in a Chinese population, Gene 678 (2018) 49–54.
[71] Loci associated with ischaemic stroke and its subtypes (SiGN): a genome-wide association study, Lancet Neurol. 15 (2) (2016) 174–184.
[72] Q. Mu, et al., Transcriptomic profiling reveals the antiapoptosis and antioxidant stress effects of Fos in ischemic stroke, Front. Neurol. 12 (2021), 728984.
[73] S.L. Mehta, et al., Long noncoding RNA Fos downstream transcript is developmentally dispensable but vital for shaping the poststroke functional outcome, Stroke 52 (7) (2021) 2381–2392.
[74] J.J. Ashbaugh, et al., IL7Rα contributes to experimental autoimmune encephalomyelitis through altered T cell responses and nonhematopoietic cell lineages, J. Immunol. 190 (9) (2013) 4525–4534.
[75] C.Y. Liao, et al., A novel pathogenic mutation on Interleukin-7 receptor leading to severe combined immunodeficiency identified with newborn screening and whole exome sequencing, J. Microbiol. Immunol. Infect. 53 (1) (2020) 99–105.
[76] X. Wang, et al., Is immune suppression involved in the ischemic stroke? A study based on computational biology, Front. Aging Neurosci. 14 (2022), 830494.
[77] A. Nyamsambuu, et al., Molecular mechanism of inhibitory effects of melatonin on prostate cancer cell proliferation, migration and invasion, PLoS One 17 (1) (2022), e0261341.
[78] H. Xu, et al., Lentivirus-mediated overexpression of OTULIN ameliorates microglia activation and neuroinflammation by depressing the activation of the NF-κB signaling pathway in cerebral ischemia/reperfusion rats, J. Neuroinflammation 15 (1) (2018) 83.
[79] Y. Ren, et al., Spata2 knockdown exacerbates brain inflammation via NF-κB/P38MAPK signaling and NLRP3 inflammasome activation in cerebral ischemia/reperfusion rats, Neurochem. Res. 46 (9) (2021) 2262–2275.